THE JOURNAL OF PHYSICAL CHEMISTRY B

Article

Cite This: J. Phys. Chem. B 2018, 122, 3426−3440

pubs.acs.org/JPCB

On the Density Dependence of the Integral Equation Coarse-Graining Effective Potential

Mohammadhasan Dinpajooh and Marina G. Guenza*

Department of Chemistry and Biochemistry, and Institute of Theoretical Science, University of Oregon, Eugene, Oregon 97403, United States

Supporting Information

ABSTRACT: Coarse-graining (CG) procedures provide computationally efficient methods for investigating the corresponding long time- and length-scale processes. In the bottom-up approaches, the effective interactions between the CG sites are obtained using the information from the atomistic simulations, but reliable CG procedures are required to preserve the structure and thermodynamics. In this regard, the integral equation coarse-graining (IECG) method is a promising approach that uses the first-principles Ornstein−Zernike equation in liquid state theory to determine the effective potential between CG sites. In this work, we present the details of the IECG method while treating the density as an intrinsic property and active variable of the CG system. Performing extensive simulations of polymer melts, we show that the IECG theory/simulation and atomistic simulation results are consistent in structural properties such as the pair-correlation functions and form factors, and also thermodynamic properties such as pressure. The atomistic simulations of the liquids show that the structure is largely sensitive to the repulsive part of the potential. Similarly, the IECG simulations of polymeric liquids show that the structure can be determined by the relatively short-range CG repulsive interactions, but the pressure is only accurately determined once the long-range, weak CG attractive interactions are included. This is in agreement with the seminal work by Widom on the influence of the potential on the phase diagram of the liquid [Widom, B. *Science* **1967**, *157*, 375−382]. Other aspects of the IECG theory/simulations are also discussed.

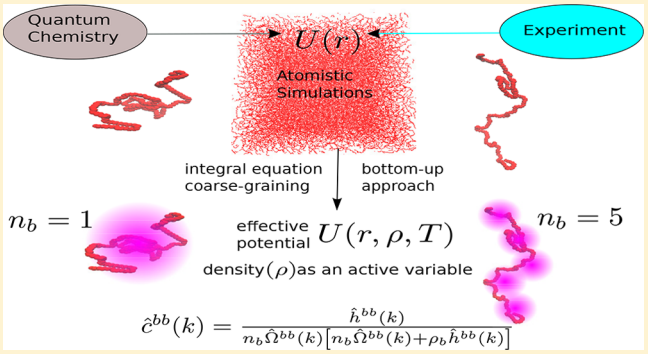

1. INTRODUCTION

Many interesting properties in macromolecule liquids depend on the chain length, N, such as phase separation, demixing, self-assembly, and glass transition temperature,[1] which have different time and length scales. Computer simulations allow one to explore essential properties and fundamental mechanisms of the polymeric systems, but atomistic simulations are not close to representing common polymeric systems,[2] which have large N, because they are computationally expensive. This is true even for simulations of the phenomena involving relatively short time scales such as relaxation of the polymer melts[3] with only a small number of chains, where significant finite size effects exist. Therefore, reliable coarse-graining (CG) representations are very much required to speed up the simulations by eliminating the microscopic degrees of freedom.

The CG models can adopt either top-down or bottom-up approaches. In the top-down approach, a set of experimental data is directly used to obtain the CG parameters, while in the bottom-up approaches the CG parameters are, in principle, obtained from the underlying atomistic simulations.[4] Well-known bottom-up approaches are the Iterative Boltzmann Inversion (IBI)[5] and Force Matching procedures.[6] Hybrid approaches have also been developed that combine both bottom-up and top-down strategies.[7] Most CG models fail to simultaneously reproduce all properties accurately even at the thermodynamic state of calibration, which is known as the so-called representability problem.[8] In addition, the accuracy of the CG parameters optimized for a set of thermodynamic states is only limited to state points close to the calibration state and does not apply to other thermodynamic conditions, which is known as the transferability problem.[9] Furthermore, recognition of the CG sites may be performed by mapping procedures, which involve different strategies such as simple mapping of the CG sites onto the center-of-mass or center-of-charge of the underlying groups of atoms. More sophisticated mapping procedures may involve performing principal component analysis or elastic network models to determine localized fluctuations and coarse-graining the atoms with analogous behavior.[10]

No matter how the CG procedure is performed, the number of degrees of freedom is reduced and care is required to interpret the properties of the CG model. In particular, the potential between the CG sites is a free energy, and many aspects of state-dependent potentials apply to effective CG potentials.[11−13]

Special Issue: Benjamin Widom Festschrift

Received: October 23, 2017
Revised: November 15, 2017
Published: November 16, 2017

DOI: 10.1021/acs.jpcb.7b10494
J. Phys. Chem. B 2018, 122, 3426−3440

When the effective CG potential has explicit density and/or temperature dependencies, the density and/or temperature are regarded as active variables of the system, and the usual statistical-mechanical expressions for energy, pressure, and isothermal compressibility require fundamental changes.

A promising approach to solve the aforementioned representability and transferability problems is to perform the coarse-graining strictly based on the Ornstein−Zernike equation[14] in the liquid state theory. The integral equation theories[15] warrant the proper calculation of the effective interactions between CG sites, which emerge from the propagation through the liquid of the many-body atomistic interactions. In this regard, the Integral Equation Coarse-Graining (IECG) method is developed in our group, where the CG sites (blobs) are larger than the polymer persistence length. The mapping procedure involves identifying the center-of-mass of the underlying groups of atoms, which allows one to relate the monomer−monomer structural correlations to the blob−blob structural correlations.[16−18] The IECG method was successfully applied to polymeric liquids when the density was treated as a passive variable of the system and accurately described both structure and thermodynamic properties.[19−22] The corresponding effective CG potentials were characterized by soft potentials with long-range repulsive tails and, at even larger distances, very shallow attractive wells. Considering the range of CG interactions, here we attribute the repulsive part of the effective CG potential as relatively short-range and the attractive part as relatively long-range.

In this work, we present the IECG method from a bottom-up approach perspective when the density is treated as an active variable of the system. This means that the potential changes as the total density fluctuates. We investigate the density dependence of the effective CG potential and its corresponding CG virial and test the compatibility of the CG and atomistic virials. The implications of temperature dependence for effective CG potential will be reserved for later consideration. We also discuss the role of relatively short-range repulsive and relatively long-range weak attractive CG interactions on structural and thermodynamic properties. In particular, we address under what circumstances two different effective CG potentials generate almost indistinguishable pair correlations.

The remainder of the paper is organized as follows: in the next section, the IECG theory is discussed in detail. In Section 3, the IECG method is demonstrated for soft spheres and multiblobs. This is done for both the IECG theory and the IECG simulations. Next, the transferability of the IECG method is discussed. In Section 5, the results of IECG simulations are discussed when the effective CG potential is truncated with different approaches. This is followed by discussion and conclusions.

2. IECG THEORY

Many aspects of the IECG theory are already described extensively in a number of our publications.[19−22] This section formulates the IECG theory from the perspective of a formal statistical-mechanical theory while briefly presenting the aspects of the IECG theory previously discussed. The IECG theory is a coarse-graining theory based on the solution of the Ornstein−Zernike integral equation,[23] extended to macromolecular liquids.[1,24] In the IECG model, each polymer in the melt is described as a chain of CG units, positioned at a distance along the chain comparable to or larger than the persistence length.[25] As shown in Figure 1 each polymer is partitioned into a number, n_b, of blobs or CG units. In the case where $n_b = 1$, the polymer is described as a point particle interacting with a soft potential, i.e.,

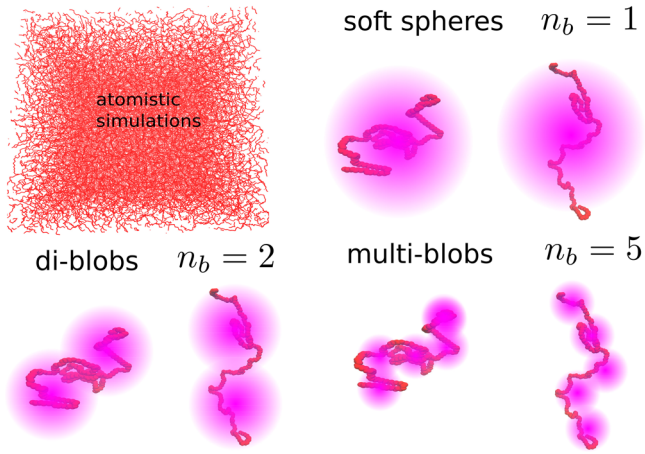

Figure 1. Top left shows a snapshot of typical atomistic molecular dynamics simulations. The top right displays two polymer chains consisting of 300 monomers, which are represented by soft spheres. The bottom left and right display two polymer chains consisting of 300 monomers, which are represented by diblobs and five blobs, respectively.

the soft sphere model. However, it is of great importance to be able to treat the same molecular system at different resolutions in multiscale modeling. Low resolution CG methods usually allow one to extremely enhance the computational speed, while higher resolution CG methods give a more detailed description of the structure on the local-scale, which is necessary to study the properties of aggregation, interaction with surfaces, and self-assembly of macromolecules. Therefore, the IECG theory may be used to describe higher resolution modeling, which involves representing the polymer as more than one blob. In soft sphere or multiblob representations, each blob represents a number of monomers, N_b, such that the total number of monomers in a chain is $N = n_b N_b$.

2.1. Effective Hamiltonian. The effective Hamiltonian of the polymer melts, H, represented by one or more blobs, is given by

$$H = K + U^{\text{intra}} + U^{\text{inter}} \tag{1}$$

where K, U^{intra}, and U^{inter} are the total kinetic, effective intramolecular, and effective intermolecular energies.

When the polymer is represented as more than one blob, these are treated as flexible without rigid constraints.[26] The blobs may be considered as point masses, and the kinetic energy of the system is given by

$$K = \sum_{k=1}^{nn_b} \sum_{a=1}^{3} \frac{p_{ka}^2}{2m_{bk}} \tag{2}$$

where n is the number of polymers, n_b is the number of blobs in a given polymer, and $a = 1, 2, 3$ designates the component of the Cartesian coordinates of the kth blob with a momentum of p_a and mass of m_b.

The classical configuration integral of the system[14,27] may be written by

$$Z = \int \dots \int e^{-\beta(U^{\text{intra}}+U^{\text{inter}})}\, d\mathbf{r} \tag{3}$$

where β is inverse temperature, $d\mathbf{r} = \prod_{i=1}^{n}\prod_{\gamma=1}^{n_b} d\mathbf{r}_i^{\gamma}$, and U^{inter} is taken to be a sum of pairwise interactions (see eq 14). Therefore, the corresponding canonical partition function in this classical approximation is given by

DOI: 10.1021/acs.jpcb.7b10494
J. Phys. Chem. B 2018, 122, 3426−3440

$$Q = \frac{Z}{\Lambda^{3nn_b} n!} \tag{4}$$

where $\Lambda = (2\pi\beta\hbar^2/m_b)^{1/2}$, the mean thermal de Broglie wavelength.

The total intramolecular effective potential is given by

$$U^{intra} = U^{bond} + U^{angle} + U^{nb} \tag{5}$$

where U^{bond}, U^{angle}, and U^{nb} are the total effective bond potential between intrachain blobs in the field of the surrounding polymer chains, total effective angle potential, and total effective nonbonded intrachain potential between the blobs that are separated more than two apart,[19] respectively. Note that, as the level of CG decreases, dihedral angles might be necessary to incorporate in the model, but in this work we are only concerned with the relatively high levels of CG and very soft potentials. Making use of an appropriate Jacobian determinant,[27,28] one may use the relative coordinates to describe the aforementioned effective potentials. The total effective bond potential is then given by

$$U^{bond} = \sum_{i}^{n} \left[\sum_{\gamma}^{n_b-1} 2n_b k_B T l_{i\gamma}^2 / \langle R^2 \rangle + k_B T \ln(g^{bb}(l_{i\gamma})) + U_{eff}^{bb}(l_{i\gamma}) \right] \tag{6}$$

where l, k_B, T, and $\langle R^2 \rangle$ are the bond length between blobs, the Boltzmann constant, temperature, and the mean-square end-to-end distance, respectively. As can be seen, an intermolecular term, obtained by subtracting the potential of mean force from the effective intermolecular potential U_{eff}^{bb}, is added to the bond potential, where g^{bb} is the radial distribution function (RDF) between blobs. This intermolecular term is designed to reproduce the appropriate bond length distribution.

The total effective angle potential is given by

$$U^{angle} = \sum_{i}^{n} \left[\sum_{\xi}^{n_b-2} -k_B T \ln[P(\theta_{i\xi})/\sin(\theta_{i\xi})] \right] \tag{7}$$

where the angular probability distribution for a random walk chain is given by

$$P(\theta) = \frac{(1-a^2)^{3/2} \sin\theta}{\pi(1-a^2\cos^2\theta)^2} \left[\frac{1 + 2a^2\cos^2\theta \arccos(-a\cos\theta)}{\sqrt{1-a^2\cos^2\theta}} + 3a\cos\theta \right] \tag{8}$$

with $a \to -0.25$ for long chains.[29]

Now we discuss how the intermolecular effective potential, U_{eff}^{bb}, is obtained in the IECG method, where each blob consists of a large enough number of monomers so that one can use Gaussian statistics to obtain the intramolecular correlations. A 2 × 2 matrix Ornstein–Zernike (OZ) equation[14,16,17,23] is first solved for a system consisting of the monomer sites and the blob sites to get the total blob–blob correlation function, h^{bb}. It is assumed that there is no direct correlation between the monomer–blob sites and also blob–blob sites. Therefore, one can relate h^{bb} to the total monomer–monomer, h^{mm}

$$\hat{h}^{bb}(k) = \left[\frac{\hat{\Omega}^{bm}(k)}{\hat{\Omega}^{mm}(k)} \right]^2 \hat{h}^{mm}(k) \tag{9}$$

where $\hat{\Omega}^{mm}(k)$ and $\hat{\Omega}^{bm}(k)$ are the normalized monomer–monomer and blob–monomer form factors given below, respectively. They characterize the internal structure of polymers and are related to the Fourier components of the intramolecular monomer density.

The total monomer correlation function, $\hat{h}^{mm}(k)$, is then estimated in Fourier space by the polymer reference interaction site model (PRISM)[1,24] for a homopolymer fluid

$$\hat{h}^{mm}(k) = \frac{\hat{\omega}^{mm}(k)^2 \hat{c}^{mm}(k)}{1 - \rho_m \hat{\omega}^{mm}(k)\hat{c}^{mm}(k)} \tag{10}$$

where $\hat{\omega}^{mm}(k) = N\hat{\Omega}^{mm}(k)$, N is the number of monomers in the polymer, ρ_m is the number density of monomer sites, and $\hat{c}^{mm}(k)$ is the monomer direct correlation function.

Noting that, at relatively large distances, the monomer direct correlation function is almost constant in Fourier space, one can approximate $\hat{c}^{mm}(k) = \hat{c}^{mm}(0) = c_0$:

$$\hat{h}^{bb}(k) = \frac{c_0 \hat{\omega}^{bm}(k)^2}{1 - \rho_m c_0 \hat{\omega}^{mm}(k)} \tag{11}$$

where $\hat{\omega}^{bm}(k) = N\hat{\Omega}^{bm}(k)$, and c_0 has density, temperature, and N dependencies.

The direct correlation function between blob sites, $\hat{c}^{bb}(k)$, is determined by solving the OZ equation for a system consisting of only blob sites:

$$\hat{c}^{bb}(k) = \frac{\hat{h}^{bb}(k)}{n_b \hat{\Omega}^{bb}(k)[n_b \hat{\Omega}^{bb}(k) + \rho_b \hat{h}^{bb}(k)]} \tag{12}$$

where n_b is the number of blobs, and ρ_b is the number density of blobs.

The effective CG potential for a pair of blobs is finally obtained by making use of an appropriate closure, such as the hypernetted chain (HNC) closure[30] that works well for the soft bounded potentials and in the limits of interest, i.e., melt density and long chains:

$$\beta U_{eff}^{bb}(r, \rho_c, T, N) = -\ln[h^{bb}(r, \rho_c, T, N) + 1] + h^{bb}(r, \rho_c, T, N) - c^{bb}(r, \rho_c, T, N) \tag{13}$$

Note that the closure, together with the OZ equation, implicitly captures the many-body effects.[31,32] Therefore, the total effective intermolecular (nonbonded) interaction in eq 3 is given by

$$U^{inter} = \sum_{i}^{n-1} \sum_{j>i}^{n} \sum_{\gamma}^{n_b} \sum_{\alpha}^{n_b} U_{eff}^{bb}(r_{ij}^{(\gamma\alpha)}, \rho_c, T, N) \tag{14}$$

where the Greek indices are used to label the number of a blob along a chain.

Hence, the IECG effective potential can be used as an input to existing software programs for Molecular Dynamics (MD) and Monte Carlo (MC) simulations as discussed below.

2.2. Soft Spheres: Equation of State. Here we discuss the equation of state (EOS), when the density is an active variable of the soft sphere system.[12] The EOS may be obtained from

DOI: 10.1021/acs.jpcb.7b10494
J. Phys. Chem. B 2018, 122, 3426–3440

$$P = k_B T\left(\frac{\partial \ln Z}{\partial V}\right)_{n,T} \tag{15}$$

where P and V are the pressure and volume of the system. The resulting pressure is obtained as

$$\frac{P}{\rho_c k_B T} = 1 - \frac{2\pi\rho_c}{3k_B T}\int_0^\infty r^3 g^{cc}(r, \rho_c, T, N)\frac{\partial U_{eff}^{cc}(r, \rho_c, T, N)}{\partial r}\,dr + \frac{2\pi\rho_c^2}{k_B T}\int_0^\infty r^2 g^{cc}(r, \rho_c, T, N)\frac{\partial U_{eff}^{cc}(r, \rho_c, T, N)}{\partial \rho_c}\,dr \tag{16}$$

where g^{cc} and U_{eff}^{cc} are the RDF and the effective density-dependent potential energy between the soft spheres. In what follows, the superscript cc is used to indicate the correlation/potential between the soft spheres.

An analytical solution of eq 16 can be derived making use of the mean-spherical approximation (MSA) closure and $g^{cc}(r, \rho_c, T, N) = 1$. Note that the MSA closure can be derived formally from the HNC closure by assuming that the pair distribution function is equal to 1, and that the use of the MSA is well-justified for polymer melts of high density, where the CG potential has a long-range, slowly varying tail. This approximation gives the soft sphere EOS as

$$\frac{P}{\rho_c k_B T} = 1 - \frac{\rho_m N c_0^{eff}(\rho_m, T, N)}{2} \tag{17}$$

where $c_0^{eff}(\rho_m, T, N) = (c_0(\rho_m, T, N) + \rho_m \partial c_0(\rho_m, T, N)/\partial\rho_m)$ (see the Supporting Information (SI) for details).

The direct correlation function between soft spheres in the reciprocal space is then obtained as

$$c_{eff}^{cc}(k) = -\frac{N\Gamma^{eff}}{\rho_m}\frac{\Omega^{cm}(k)^2}{1 + \Gamma^{eff}(\Omega^{mm}(k) - \Omega^{cm}(k)^2)} \tag{18}$$

where $\Gamma^{eff} = \Gamma + \Gamma_\rho$ with $\Gamma = -N\rho_m c_0$ and $\Gamma_\rho = -N\rho_m^2 \partial c_0/\partial\rho_m$. The monomer intramolecular distribution is given by the Debye function

$$\hat{\Omega}^{mm}(k) = \frac{2(e^{-q} + q - 1)}{q^2} \tag{19}$$

where $q = k^2\langle R^2\rangle/6$, and the monomer-cm distribution is given by

$$\hat{\Omega}^{cm}(k) = \frac{\sqrt{\pi}}{q^{1/2}} e^{-q/12}\,\mathrm{erf}\left[\frac{q^{1/2}}{2}\right] \tag{20}$$

An inverse Fourier transform of $c_{eff}^{cc}(k)$ while keeping the leading term results in

$$c_{eff}^{cc(0)}(r, T, \rho_c, N) = -\frac{B(\Gamma^{eff})^{1/2}}{r}\sin\left[\frac{Dr}{(\Gamma^{eff})^{1/4}}\right] e^{-Dr/(\Gamma^{eff})^{1/4}} \tag{21}$$

where $B = \frac{9\sqrt{5}}{2\pi\rho_c\langle R^2\rangle}$ and $D = 3\sqrt{\frac{5^{1/2}}{\langle R^2\rangle}}$. It is useful to stress that this direct correlation function incorporates the density dependence of the CG virial, which allows one to obtain the CG pressure in MSA as

$$\frac{P}{\rho_c k_B T} = 1 + \frac{2\pi\rho_c}{3}\int_0^\infty r^3 g_{CG}^{cc}(r)\frac{\partial c_{eff}^{cc(0)}(r, \rho_c, T, N)}{\partial r}\,dr \tag{22}$$

where $g_{CG}^{cc}(r)$ denotes that the RDF has temperature, density, and N dependencies (see SI for the detailed derivations). By assuming $g_{CG}^{cc}(r) = 1$, eq 22 reduces to eq 17, which may be written as

$$\frac{P}{\rho_c k_B T} = 1 + \frac{\Gamma^{eff}}{2} \tag{23}$$

with $\Gamma^{eff} = -\rho_m N c_0^{eff}(\rho_m, T, N)$. This indicates that when the monomer (atomistic) configurations are mapped into the CG configurations, another contribution may be added to c_0, which captures the volume dependence of the effective CG interactions. Therefore, in the IECG theory the CG pressure for soft spheres may be obtained by a simple EOS

$$\frac{P}{\rho_c k_B T} = 1 - \frac{2\pi\rho_c}{3k_B T}\int_0^\infty r^3 g_{CG}^{cc}(r)\frac{\partial U_{CG}^{cc}(r, \rho_c, T, N)}{\partial r}\,dr \tag{24}$$

where U_{CG}^{cc} is the effective CG potential, which incorporates the density dependence of the CG virial through c_0^{eff}. Note that various closures such as MSA or HNC may be used to obtain U_{CG}^{cc} in eq 24. This equation, with the HNC closure, is used when reporting the IECG theoretical values of pressure. As will be shown in Section 3, the resulting effective CG potential accurately reproduces the pair-correlation functions.

2.3. Multiblobs: Equation of State. The pressure (EOS) for multiblobs may be obtained using eq 15, which results in decomposing the pressure into kinetic and intramolecular and intermolecular contributions as

$$P = P_{kin} + P_{inter} + P_{intra} \tag{25}$$

where each term is presented in detail below.

The kinetic contribution is obtained as

$$P_{kin} = \rho_b k_B T \tag{26}$$

The intermolecular contribution is obtained as

$$P_{inter} = -\frac{2\pi\rho_b^2}{3}\int_0^\infty r^3 g_{CG}^{bb}(r)\frac{\partial U_{CG}^{bb}(r, \rho_c, T, N)}{\partial r}\,dr \tag{27}$$

where the effective CG potential, U_{CG}^{bb}, is calculated through c_0^{eff} by making use of the normalized monomer−monomer $\hat{\Omega}^{mm}$, blob−monomer $\hat{\Omega}^{bm}$, and blob−blob $\hat{\Omega}^{bb}$ intramolecular form factors. The normalized monomer−monomer intramolecular form factors for multiblobs in the blob averaged limit may be written as

$$\hat{\Omega}^{mm}(k) = \frac{2}{n_b^2 q_b^2}(q_b n_b - 1 + e^{-n_b q_b}) \tag{28}$$

where $q_b = q/n_b$, and $q = k^2\langle R^2\rangle/6$ and $\hat{\Omega}^{mm}(k) = \hat{\omega}^{mm}(k)/N$. The normalized blob−monomer intramolecular form factors are given by

DOI: 10.1021/acs.jpcb.7b10494
J. Phys. Chem. B 2018, 122, 3426−3440

$$\hat{\Omega}^{\mathrm{bm}}(k) = \frac{1}{n_b}\left[\frac{\sqrt{\pi}}{q_b^{1/2}}\mathrm{erf}\left(\frac{q_b^{1/2}}{2}\right)e^{-q_b/12} - 2\left(\frac{e^{-n_b q_b} - n_b e^{-q_b} + n_b - 1}{n_b q_b(e^{-q_b} - 1)}\right)e^{-q_b/3}\right] \quad (29)$$

where $\hat{\Omega}^{\mathrm{bm}}(k) = \hat{\omega}^{\mathrm{bm}}(k)/N$. The following normalized blob−blob intramolecular form factors are used

$$\hat{\Omega}^{\mathrm{bb}}(k) = \frac{1}{n_b} + 2\left[\frac{e^{-n_b q_b} - n_b e^{-q_b} + (n_b - 1)}{n_b^2(e^{-q_b} - 1)^2}\right]e^{-2q_b/3} \quad (30)$$

where $\hat{\Omega}^{\mathrm{bb}}(k) = \hat{\omega}^{\mathrm{bb}}(k)/n_b$.

The intramolecular contribution of the pressure consists of the harmonic part of the bond interactions, P_b^{harm}, the repulsive part of the bond interactions, P_b^{rep}, and the nonbonded interactions, P_{nb}:

$$P_{\mathrm{intra}} = P_b^{\mathrm{harm}} + P_b^{\mathrm{rep}} + P_{\mathrm{nb}} \quad (31)$$

The pressure due to harmonic bond interactions is obtained as

$$P_b^{\mathrm{harm}} = -\frac{4\pi\rho_c(n_b - 1)}{3}\int_0^\infty r^3\omega_{\mathrm{CG}}^{\mathrm{bb1}}(r)\frac{\partial U_b^{\mathrm{harm}}(r, \rho_c, T, N)}{\partial r}\,\mathrm{d}r \quad (32)$$

with $U_b^{\mathrm{harm}} = 9n_b k_B T r^2/(4\langle R^2\rangle)$, and $\omega_{\mathrm{CG}}^{\mathrm{bb1}}$, the blob−blob bond length distribution, as

$$\omega_{\mathrm{CG}}^{\mathrm{bb1}}(r) = \left(\frac{3}{8\pi}\right)^{3/2}\frac{e^{-18n_b r^2/\langle R^2\rangle}}{(\langle R^2\rangle/(6n_b))^{3/2}} \quad (33)$$

It is worth mentioning that the contribution from the harmonic bonds can be integrated analytically and combined with the kinetic contributions to give

$$P_{\mathrm{kin}} + P_b^{\mathrm{harm}} = \rho_c k_B T \quad (34)$$

suggesting that the kinetic and harmonic bond contributions in the multiblob models can compensate for each other.

The pressure due to the repulsive part of bond interactions is obtained as

$$P_b^{\mathrm{rep}} = -\frac{4\pi\rho_c(n_b - 1)}{3}\int_0^\infty r^3\omega_{\mathrm{CG}}^{\mathrm{bb1}}(r)\frac{\partial U_b^{\mathrm{rep}}(r, \rho_c, T, N)}{\partial r}\,\mathrm{d}r \quad (35)$$

with

$$U_b^{\mathrm{rep}} = U_{\mathrm{CG}}^{\mathrm{bb}}(r) + k_B T\ln(g_{\mathrm{CG}}^{\mathrm{bb}}(r)) \quad (36)$$

The pressure due to the intramolecular nonbonded interactions between the blobs, which are more than two apart, is obtained as

$$P_{\mathrm{nb}} = -\frac{4\pi\rho_c}{3}\int_0^\infty r^3\omega_{\mathrm{CG}}^{\mathrm{bb>3}}(r)\frac{\partial U_{\mathrm{CG}}^{\mathrm{bb}}(r, \rho_c, T, N)}{\partial r}\,\mathrm{d}r \quad (37)$$

with

$$\omega_{\mathrm{CG}}^{\mathrm{bb>3}}(k) = \frac{e^{-8/3q_b}(n_b - 3) + e^{-(2+3n_b)/3q_b} - e^{-11/3q_b}(n_b - 2)}{(1 - e^{-q_b})^2} \quad (38)$$

where $q_b = q/n_b$.

As will be shown in the next section, the multiblob EOS in the IECG theory works reasonably well when compared to the atomistic and IECG simulation results.

3. DEMONSTRATION OF THE IECG METHOD: MOLECULAR DYNAMIC SIMULATIONS

In this section, we demonstrate the IECG method for soft spheres and multiblobs for various degrees of polymerization at a density of 0.77 g/cm^3 at 503.17 K and discuss how it can be mapped into atomistic simulations. We would like to stress that the IECG method may be used in the top-down or bottom-up approaches. When the bottom-up approach is used, only a few atomistic simulations are required to set the parameters of the formalism (c_0^{eff} and $\langle R^2\rangle$), and this is verified in Section 4.

3.1. Atomistic Simulation Details. A detailed description of the atomistic MD simulation protocols is given in the SI. Here, we only briefly present them. The atomistic simulations were performed using the LAMMPS software program[33] in the canonical ensemble at the corresponding state points. A Nosé−Hoover thermostat and standard velocity-Verlet integrator were used for the atomistic simulations with a time step of 1.25 fs. A cutoff distance of 14 Å was used, where both potential and force were required to go smoothly to zero at the cutoff distance by multiplying the potential by the Mei−Davenport−Fernando taper function.[34] The equilibration period ranged from 10 to 50 ns, and the production period consisted of 45−160 ns for various polymer melts as discussed in the SI.

3.2. IECG Simulation Details. All IECG MD simulations were performed in the canonical ensemble with a Nosé−Hoover thermostat with a standard velocity-Verlet integrator. The end-to-end distance and c_0^{eff} reported in Table 1 were used. Note that eq 17 has been used to obtain the values of c_0^{eff} for the IECG simulations. The cutoff distances for the IECG simulations were determined over the range of $r > 0$ from the location of the second extremum of the effective CG potential, i.e., 186, 290, 348, and 391 Å for soft sphere simulations of polymers with the degrees of polymerization, N, of 96, 192, 250, and 300,

Table 1. Top: Mean-Square End-to-End Distance $\langle R^2\rangle$, Mean-Square Radius-of-Gyration R_g^2, Pressure P, and c_0^{eff} Obtained Directly from a Few Atomistic Simulations of Polymer Melts with Various Degrees of Polymerizations, N[a]

Atomistic Simulations				
N	$\langle R^2\rangle/6$, Å^2	R_g^2, Å^2	P, atm	c_0^{eff}, Å^3
96	293 ± 7	265 ± 4	523 ± 7	−13.5 ± 0.2
192	610 ± 16	580 ± 11	393 ± 6	−10.2 ± 0.2
250	815 ± 33	784 ± 20	362 ± 5	−9.5 ± 0.1
300	969 ± 29	943 ± 16	343 ± 4	−9.0 ± 0.1
Soft Spheres: IECG Simulations/Theory				
N	$P_{\mathrm{simulations}}$, atm	P_{theory}, atm	P_{MSA}, atm	
96	523 ± 1	523	524	
192	392 ± 1	392	392	
250	362 ± 1	361	362	
300	343 ± 1	343	344	

[a]The statistical uncertainties are the standard deviations obtained from block averages. Note that $\langle R^2\rangle/6$ relatively deviates less from R_g^2 for longer chains. Bottom: The values of pressure obtained from the IECG simulations and compared with the IECG theory (eq 24). For comparison, the values of pressure are also reported when the mean-spherical approximation (MSA) and $g^{cc} = 1$ approximation are applied to eq 24, P_{MSA}.

DOI: 10.1021/acs.jpcb.7b10494
J. Phys. Chem. B 2018, 122, 3426−3440

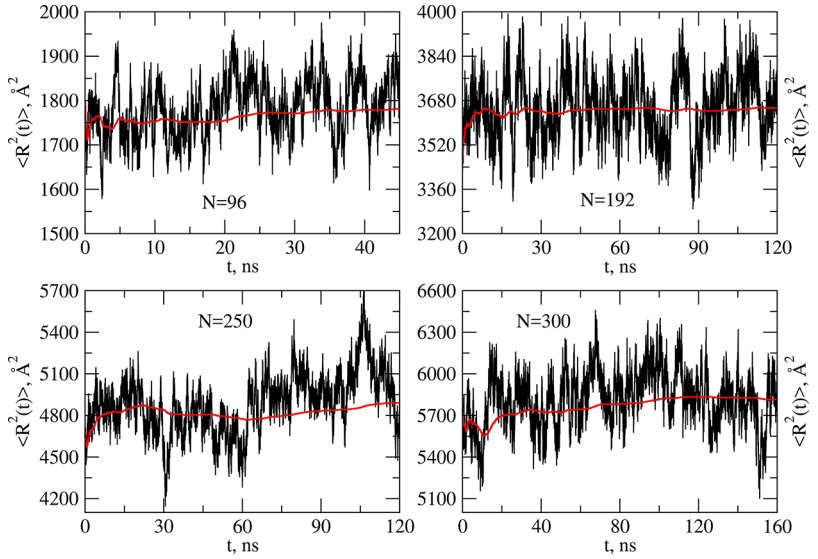

Figure 2. Evolution of the instantaneous average end-to-end distance (black lines) obtained for the production period of atomistic simulations of polymers with degrees of polymerization N of 96 (top left panel), 192 (top right panel), 250 (bottom left panel), and 300 (bottom right panel). The atomistic simulations for $N = 96$ and 192 consisted of 350 polymer chains, while the atomistic simulations for $N = 250$ and 300 consisted of 300 polymer chains. The red lines show the cumulative mean-square end-to-end distance at a given MD step.

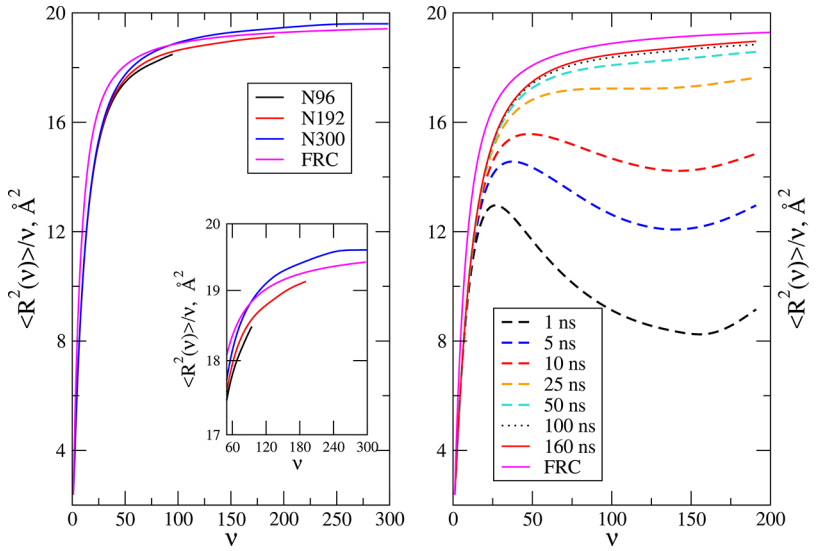

Figure 3. Left panel: mean-square internal distances from long MD runs for atomistic simulations of polymers with degrees of polymerization N of 96 (black), 192 (red), and 300 (blue). Right panel: evolution of the mean-square internal distances from long MD runs for atomistic simulations of polymers with degrees of polymerization N of 192. In both panels, the magenta line shows the theoretical predictions of a freely rotating chain model.

respectively. A neighbor skin distance of 2 Å, a simulation parameter that determines the Verlet neighbor lists,[35] was used. In multiblob models, the time step should be smaller than the relaxation times of the fastest modes of vibration, τ, which theoretically scale as $\tau \propto n_b^{-1}$. A time step of 30 fs was used for all soft sphere, diblob, and four-blob simulations. However, for 6- and 10-blob simulations, a time step of 10 fs was used. The production runs for soft spheres consisted of 3 ns for $N = 96$ and $N = 192$ and 0.6 ns for $N = 250$ and $N = 300$. The effective CG potential becomes less long-ranged for multiblob simulations, allowing fewer force calculations in MD. For multiblobs consisting of two and four blobs, the production consisted of 3 and 30 ns, respectively. For 6- and 10-blob simulations, a production period of 10 ns was used.

3.3. Results: Consistencies in RDF, Form Factors, and Pressure. The evolution of the pressure, mean-square end-to-end distance (R^2), and mean-square radius-of-gyration (R_g^2) for a few atomistic simulations performed are shown in Figure 2 and Figures S1 and S2. The mean-square end-to-end distance and mean-square radius-of-gyration for each snapshot of the MD trajectory are defined as $\langle R^2(t)\rangle = \sum_i^n R_i^2(t)/n$ and $R_g^2(t) = \sum_i^n R_{gi}^2(t)/n$, respectively. In the atomistic simulations, the density was treated as a passive variable; i.e., the atomistic potential parameters are optimized such that they do not explicitly have density dependence. For instance, the depth of the Lennard-Jones potential is invariant to the density change. The pressure was calculated using the potential described in the SI via the virial theorem as

$$P = \langle \rho_m k_B T \rangle + \frac{\langle W \rangle}{3V} \quad (39)$$

DOI: 10.1021/acs.jpcb.7b10494
J. Phys. Chem. B 2018, 122, 3426−3440

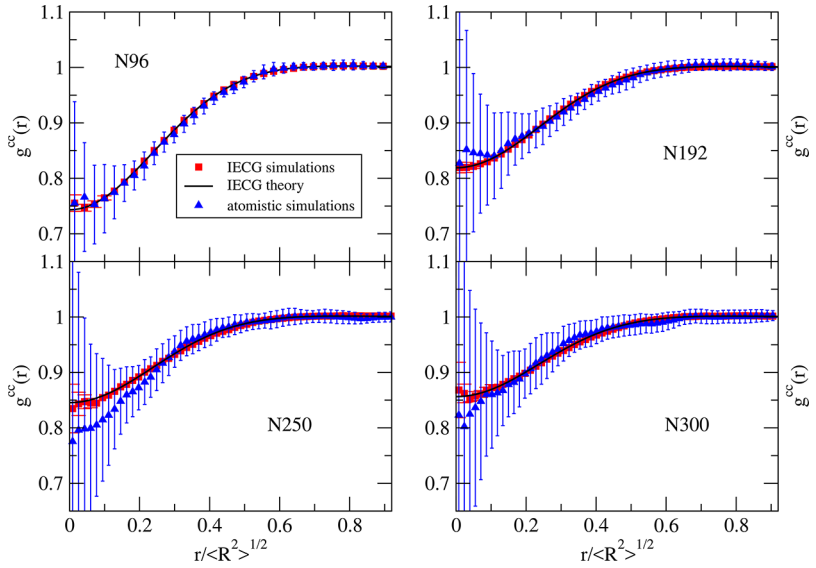

Figure 4. Theoretical and simulated radial distribution functions for polymers with degrees of polymerization, N, of 96 (top left panel), 192 (top right panel), 250 (bottom left panel), and 300 (bottom right panel) when the polymer is represented by one soft sphere. Atomistic simulation results (blue ▲) are compared with coarse-grained simulation results (red ■) and with the IECG theoretical prediction (black —). The theoretical results and the data from the coarse-grained simulations are both within the error of the atomistic simulations.

where W is the virial given in ref 36. It is worth mentioning that no explicit volume dependence exists in the atomistic virial, but an implicit volume dependence exists via scaling of r_{ij}, where r_{ij} may be calculated using the minimum-image convention for periodic systems. Note that the thermodynamic pressure was estimated by averaging the instantaneous pressure based on the kinetic energy and the atomistic virial (and not the molecular virial).

Comparing Figure S1 with Figures 2 and S2 shows that the pressure is converged relatively faster than $\langle R^2(t)\rangle$ and $R_g^2(t)$. The average values are reported in Table 1. In addition, Table 1 lists the values of c_0^{eff} obtained directly from the atomistic pressures and making use of eq 17. As will be discussed, c_0^{eff} and $\langle R^2\rangle$ are the two parameters that need to be determined in the IECG method.

The average mean-square internal distances, for a given number of internal monomers $\nu(\langle R^2(\nu)\rangle)$, were calculated to monitor the structural equilibration of the polymer melts. In atomistic simulations, it was calculated as

$$\langle R^2(\nu)\rangle = \left\langle \frac{1}{n}\sum_{i=1}^{n}\left[\frac{1}{N-\nu}\sum_{\gamma=1}^{N-\nu}(\mathbf{r}_i^{\gamma}-\mathbf{r}_i^{\gamma+\nu})^2\right]\right\rangle \tag{40}$$

where ν is the number of monomers between the γth monomer and the $(\gamma+\nu)$th monomer along the same chain. The theoretical prediction of the mean-square internal distance for a freely rotating chain (FRC) model is

$$\langle R^2(\nu)\rangle = \nu l^2\left[\frac{1-\cos\theta}{1+\cos\theta}+\frac{2\cos\theta}{(1+\cos\theta)^2}\frac{1-(-\cos\theta)^{\nu}}{\nu}\right] \tag{41}$$

where $\cos\theta = -0.785$ was used to report $\langle R^2(\nu)\rangle$ for an FRC model in Figure 3.

The left panel of Figure 3 compares $\langle R^2(\nu)\rangle$ for atomistic simulations of polymer melts with various degrees of polymerizations and the corresponding FRC model. It turns out that, for a given internal distance ν, $\langle R^2(\nu)\rangle$ from atomistic simulations is almost independent of the chain length and in close agreement with the FRC model. The right panel of Figure 3 shows the structural equilibration of the polymer melt with $N = 192$. Initially, the polymers appear to be compressed due to the artifacts introduced by the preparation procedure. The equilibration period eliminates these artifacts. Due to the strong repulsive interactions between monomers, the local monomer structure relaxes more quickly than the large-scale chain structure. No significant change in the average mean-square internal distances is observed after 50 ns.

In the IECG theory/simulations, the dimension of the polymer may be determined from the mean-square end-to-end distance, $\langle R^2\rangle$, obtained during the atomistic production period. The dimension of polymer melts with large chain lengths is usually envisaged as an ideal polymer melt in which no interactions exist aside from those responsible for chain connectivity. For the polymer melts with large N, the equality $\langle R^2\rangle/6 = R_g^2$ holds.[37] However, as shown in Table 1 for relatively short polymer melts, the atomistic simulations show significant deviations from the aforementioned equality. Considering the uncertainties in $\langle R^2\rangle$ and R_g^2, these deviations almost vanish for the polymer melt with $N = 300$.

During the coarse-graining procedure, the density becomes an active variable of the system, and the pressure was calculated using the CG effective potential as

$$P = \langle \rho_c k_B T\rangle - \frac{1}{3V}\left\langle \sum_{i}^{n-1}\sum_{j>i}^{n}\frac{dU_{CG}^{cc}(r_{ij})}{d\mathbf{r}_{ij}}\cdot\mathbf{r}_{ij}\right\rangle \tag{42}$$

which captures the density dependence as shown in eq 24. This suggests that making use of $c_0^{\text{eff}}(\rho_m, T, N)$ allows one to calculate the CG pressure without modifying the standard MD/MC codes designated for atomistic systems because the effective CG potential and force capture the density-dependent part of pressure in eq 16. The long-range CG corrections (discussed below) can be applied after NVT simulations.

Table 1 shows that the IECG simulation results lie within the statistical uncertainty of atomistic simulations. In addition, theoretical values of pressure, P_{theory}, were calculated using eq 24,

DOI: 10.1021/acs.jpcb.7b10494
J. Phys. Chem. B 2018, 122, 3426−3440

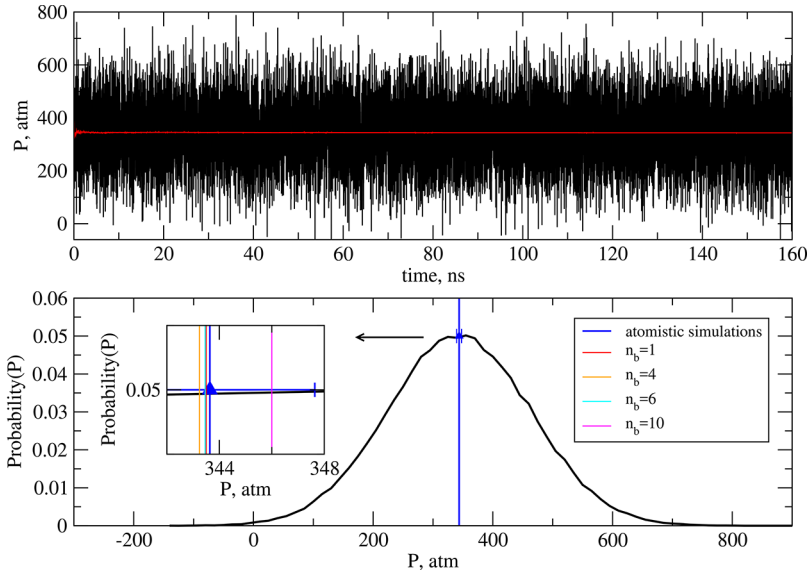

Figure 5. Top panel: evolution of the instantaneous pressure over the production run of an atomistic simulation of polyethylene with $N = 300$, at 503 K and a monomer density of 0.03296 Å^{-3} (black curve). Cumulative average pressure for the same simulation (red curve). Bottom panel: pressure distribution for the atomistic simulation (black curve). The blue line shows the average pressure for atomistic simulations with the simulation error bars obtained from block averages. The red, orange, cyan, and magenta lines show the average pressure for coarse-grained (CG) simulations with 1, 4, 6, and 10 blobs per chain, respectively. The result for two blobs is indistinguishable from the one blob representation in the plot.

and excellent agreement was observed with both the atomistic and IECG simulation results. When the MSA and $g^{cc} = 1$ approximations were applied to eq 24, it was found that the values of pressure, P_{MSA}, were also in excellent agreement with the IECG simulation/theoretical results. Figure 4 shows that the difference between the RDFs obtained by the atomistic and CG simulations is within the statistical uncertainty, and both are in excellent agreement with the IECG theoretical predictions. The RDF uncertainties in the atomistic simulations increase for longer chain polymers, which involve more conformation states, due to the lack of long enough trajectories.

Similarly, one can demonstrate the IECG method for multiblob models. The top panel of Figure 5 displays the evolution of the instantaneous atomistic pressure, P_i at step i, while the red line shows its cumulative average; for instance at step j, $\left\langle P_j \right\rangle = \frac{1}{st_j} \sum_{i=1}^{st_j} P_i$, as st_j is the number of steps up to step j. The bottom panel of Figure 5 shows in blue the probability distribution of the pressure, as obtained from the atomistic simulation, with the average pressure in blue, and the simulation error bar. The inset shows the average pressure measured in the IECG simulations, with the chains represented by 1 (red line), 4 (orange line), 6 (cyan line), and 10 (magenta line) blobs. The error bar in the blob representations is of the order of the line width. As can be seen, all the CG pressures fall within the error of the atomistic simulation.

Table 2 provides a useful analysis of the contributions to the total pressure of the polymer melt with $N = 300$ for the IECG theory and simulations. The kinetic contributions increase as the number of blobs increases, while the bonded contributions appear to significantly compensate for them. The increase in the kinetic contributions is less pronounced in the IECG simulations than the IECG theory due to a slight overestimation of the bonded contributions in the IECG theory. The nonbonded contributions are positive due to repulsive interactions between the blobs, which are more than two blobs apart and result in excellent agreement of the IECG theory/simulation results with

Table 2. Calculated Pressure with $N = 300$ When the Polymer Is Represented by Various Numbers of Blobs[a]

IECG Simulations						
n_b	$\langle P_{kin} \rangle$	$\langle P_{inter} \rangle$	$\langle P_b \rangle$	$\langle P_{nb} \rangle$	$\langle P_{vir} \rangle$	$\langle P \rangle$
1	7.5	336.0	0	0	336.0	343.5
2	15.1	335.0	−6.6	0	328.4	343.5
4	30.1	331.9	−19.2	0.4	313.1	343.2
6	45.2	328.9	−32.3	1.6	298.2	343.4
10	75.3	325.3	−59.1	4.5	270.7	346.1
IECG Theory						
n_b	$\langle P_{kin} \rangle$	$\langle P_{inter} \rangle$	$\langle P_b^{harm} \rangle$	$\langle P_b^{rep} \rangle$	$\langle P_{nb} \rangle$	$\langle P_{vir} \rangle$	$\langle P \rangle$
1	7.5	335.8	0	0	0	335.8	343.3
2	15.1	335.0	−7.5	0.7	0	328.2	343.3
4	30.1	332.2	−22.6	2.0	0.3	311.9	342.0
6	45.2	329.6	−37.7	2.9	1.6	296.4	341.6
10	75.3	326.6	−67.8	4.0	3.6	266.4	341.7

[a]In the IECG theory, P_{kin}, P_{inter}, P_b^{harm}, P_b^{rep}, and P_{nb} were obtained from eqs 26, 27, 32, 35, and 37, respectively. The atomistic pressure for this polymer melt is 343 ± 4 atm as reported in Table 1.

the atomistic ones. Although the contributions of the intramolecular nonbonded interactions between the blobs and the repulsive part of bond interactions to pressure are considerably less than other contributions for the resolutions studied in this work, they compensate for the relatively small reduction in the intermolecular pressure in higher resolution CG models leading to excellent agreement between the atomistic and IECG results. Overall, as the level of CG decreases, the virial contributions to the pressure decrease, while the kinetic contributions increase and almost compensate for them.

The left panel of Figure 6 compares the RDFs from the atomistic simulations, IECG simulations, and the IECG theory for the polymer melts of $N = 192$ represented by two blobs and $N = 300$ represented by four blobs. The difference between the IECG and atomistic simulations falls within statistical uncertainties, both of which are in excellent agreement with

DOI: 10.1021/acs.jpcb.7b10494
J. Phys. Chem. B 2018, 122, 3426−3440

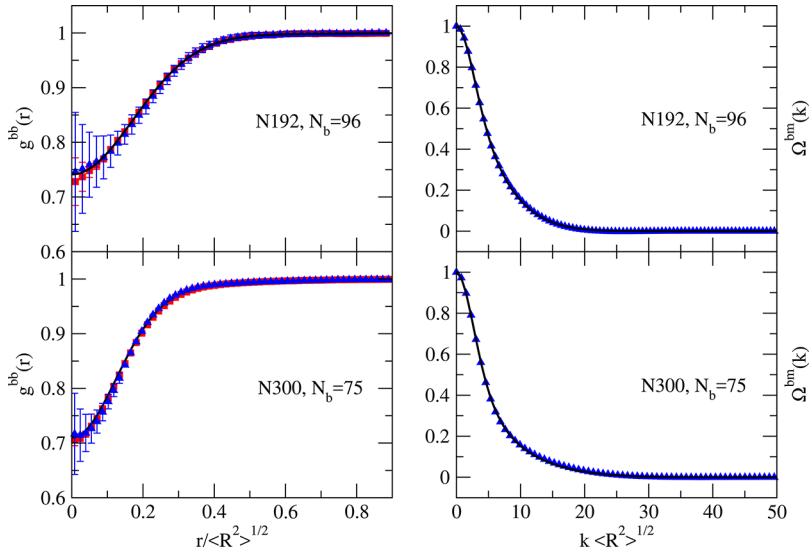

Figure 6. Left panel: IECG theoretical and simulated radial distribution functions for polymers with degrees of polymerization when the polymer is represented by two and four blobs. The atomistic simulation results (▲) are compared with the IECG simulation results (red ■) and the IECG theoretical prediction (black line). Right panel: the normalized monomer−blob form factor, Ω^{bm}, for atomistic simulations (▲) and the IECG theory (black —). The statistical uncertainties are less than the symbol size.

the IECG theory results. The right panel of Figure 6 shows excellent agreement between the normalized monomer−blob factors for polymers with $N = 192$ represented by two blobs and $N = 300$ represented by four blobs from the atomistic simulations and the IECG theory. In addition, Figures S3 and S4 also show agreement between the total correlation function and monomer−blob form factors for atomistic simulations and the IECG theory results when the polymer melt of $N = 300$ is represented by 2, 4, 6, and 10 blobs.

4. TRANSFERABILITY OF THE IECG METHOD

The common numerical CG potentials are usually optimized to reproduce an atomistic quantity at a given state point and suffer from the problem of being not transferable to other thermodynamic conditions or to other systems. However, the IECG method is transferable because it is based on analytical expressions that can determine the parameter values at state points of interest in the phase diagram. Since the focus here is on the direct mapping of the atomistic simulations to the IECG theory/simulations, a few atomistic simulations should be performed to obtain the values of c_0^{eff} and $\langle R^2 \rangle$ in the phase diagram. Accurate EOSs[1] and the principles of polymer physics[25] then allow one to easily estimate the values of these two parameters at other state points. However, if the goal of the IECG method is based on a top-down approach, i.e., making use of the experimental data for the IECG theory/simulations, then atomistic simulations may not be required as several c_0^{eff} and $\langle R^2 \rangle$ obtained from experiments are sufficient to make the IECG method transferable.

Figure 7 illustrates how the state points in the phase diagram can be determined for polymer melts with long chain lengths, where atomistic simulations are almost impractical despite access to massively parallel supercomputers. Even with a small number of chains that can have significant finite size effects, it is computationally expensive to perform atomistic simulations of chains with more than 10^5 monomers each, a reasonable chain length to study.[2] To demonstrate the transferability of the IECG method for various chain lengths, only four state points from atomistic simulations are used to determine the EOS from which

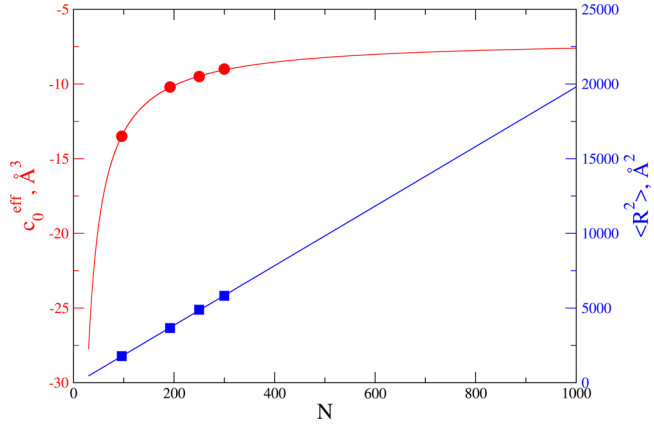

Figure 7. Values of c_0^{eff} (red ●) and $\langle R^2 \rangle$ (blue ■) computed for polymer melts of various degrees of polymerization, N, at 503 K and a monomer density of 0.03296 Å^{-3}. The red and blue solid lines are fits of the form $a + b/N$ and $a + b\,N$, respectively.

one can estimate c_0^{eff} at other state points in the phase diagram. To verify the accuracy of this procedure, independent atomistic simulations consisting of a 50 ns production period were performed for polymers with degrees of polymerization of 44, 124, and 400 at 503.17 K and a monomer density of 0.03296 Å^{-3}. No significant finite size effects were observed for these relatively short chain length polymers. For instance, the values of pressure for the polymer melt with $N = 44$ consisting of 175, 350, and 700 chains were 856 ± 12, 849 ± 11, and 853 ± 6 atm, respectively, where 20 ns was used for the equilibration period and 30 ns was used for the production period. We hesitated to report independent atomistic simulations for the polymer melts with very long chain lengths because they are computationally very expensive to equilibrate and may have more significant finite size effects given the small number of chains that is usually used in their simulations.

The top of Table 3 lists the values of pressure obtained from the IECG theory and IECG simulations in soft sphere and multiblob representations and compares them with the results

DOI: 10.1021/acs.jpcb.7b10494
J. Phys. Chem. B 2018, 122, 3426−3440

Table 3. Comparison of the Pressure from Independent Atomistic Simulations and the IECG Theory/Simulations for the Polymer Melts at 503 K at Various N (Top) and Monomer Densities (Bottom)[a]

ρ_m = 0.03296 Å^{-3}				
N	n_b	IECG theory	IECG simulations	atomistic simulations
44	1	846	846	849 ± 11
124	1	467	469	466 ± 5
124	2	467	469	466 ± 5
400	1	322	322	325 ± 4
400	2	322	322	325 ± 4
400	4	321	322	325 ± 4
400	8	320	322	325 ± 4
N = 192				
ρ_m, Å^{-3}	n_b	IECG theory	IECG simulations	atomistic simulations
0.03153	1	86	87	84 ± 4
0.03153	4	86	87	84 ± 4
0.03248	1	276	277	274 ± 5
0.03248	4	275	277	274 ± 5
0.03439	1	830	830	833 ± 4
0.03439	4	826	829	833 ± 4

[a]The IECG parameters are computed from the fits shown in Figures 7 and 9. The unit of the pressure is atm, and the uncertainties in the IECG simulations are less than 1 atm.

from independent atomistic simulations. Excellent agreement is observed between the aforementioned approaches demonstrating the transferability of the IECG method. The IECG theory in its current version tends to slightly overestimate the magnitude of bond contributions to the pressure, which resulted from the approximations related to eq 33. However, all IECG simulation results in Table 3 fall within the statistical uncertainties of atomistic simulation results showing the consistency for various levels of coarse-graining. In addition, the top panel of Figure 8 shows excellent agreement between the RDFs obtained from the aforementioned approaches for N = 44 and N = 124 (represented by two blobs). In the bottom panel of Figure 8, the probability distribution of the atomistic pressure is shown and confirms that the IECG theory/simulation results are in excellent agreement with the atomistic ones.

Similarly, the transferability of the IECG method is demonstrated at various densities for the polymer melt with N = 192 at the bottom of Table 3, where only three c_0^{eff} data points from atomistic simulations (shown in the left top panel of Figure 9) were used to determine the corresponding EOS in the phase diagram. Note that the values of $\langle R^2 \rangle$ and R_g^2 are almost constant for related densities at a given N. For instance, R_g^2 values obtained from atomistic simulations of the polymer melt with N = 192 at monomer densities of 0.03201, 0.03296, and 0.03344 Å^{-3} were found to be 577 ± 11, 580 ± 11, and 580 ± 14 Å^2. Usually, better agreements were observed between the independent atomistic simulations and the predictions/results of the IECG theory and the IECG simulations when the atomistic simulations were more converged. The equilibration period ranged from 5 to 65 ns for the data presented in Table 3 for various monomer densities and N.

4.1. Sensitivities of RDF and Pressure to c_0^{eff} and $\langle R^2 \rangle$. As discussed above, the effective CG potentials are determined in terms of c_0^{eff} and $\langle R^2 \rangle$, which are associated with uncertainties. The monomer local-scale information is captured in c_0^{eff}, while the polymer large-scale properties are included in $\langle R^2 \rangle$. To get specific local-scale information on the structural correlation functions, one may use multiscale-scale approaches as described in our previous work[38] or adaptive resolution approaches.[39]

Noting that the end-to-end distance is constant at various studied densities (as supported by the atomistic simulation results), the RDFs and effective CG potentials are presented in Figure 9 for a polymer with N = 192. The top left panel shows that the direct monomer−monomer correlations become more pronounced as the density increases. The bottom left panel

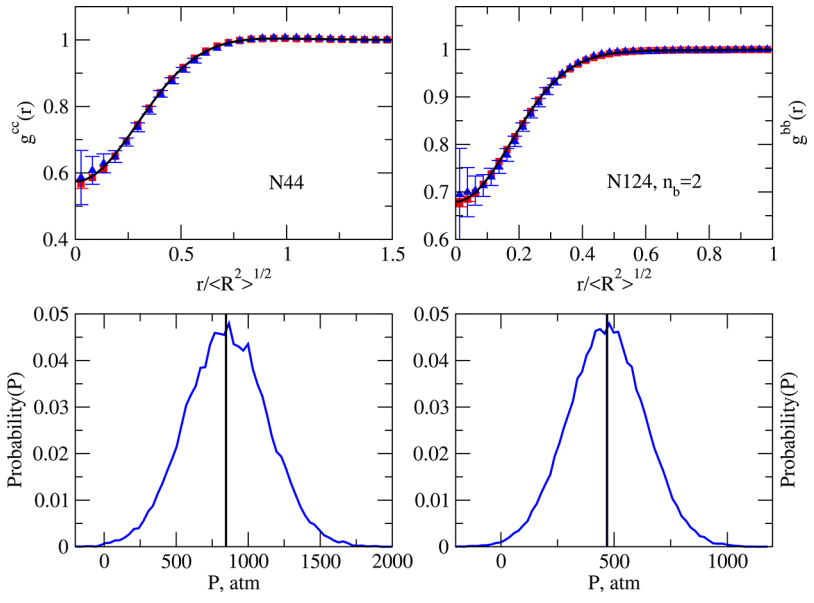

Figure 8. Top panel: comparison of RDFs obtained from independent atomistic simulations and the IECG theory for N = 44 and N = 124 at 503.17 K and a monomer density of 0.03296 Å^{-3}. The IECG theory/simulation results are within the uncertainties of independent atomistic simulation. Bottom panel: pressure distribution for the atomistic simulation (blue curve). The black line shows the pressure computed from the IECG simulations, which is indistinguishable from the independent atomistic simulation results and the IECG theory in the plot scale. See Table 3 to compare the pressure values for the aforementioned approaches.

DOI: 10.1021/acs.jpcb.7b10494
J. Phys. Chem. B 2018, 122, 3426−3440

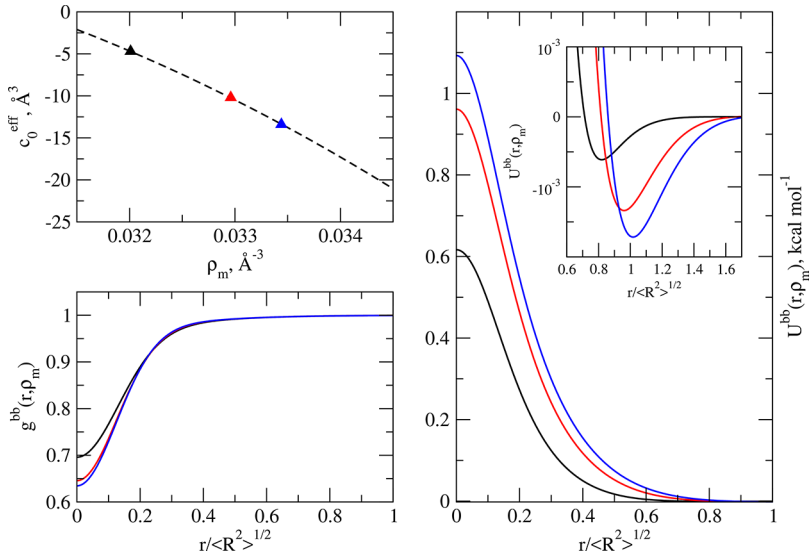

Figure 9. Top left panel: values of c_0^{eff} computed for a polymer melt with $N = 192$ at 503 K and at various monomer densities. The dashed black line is a fit to a Carnahan−Starling-type equation.[40] Bottom left panel: the radial distribution function for the polymer melt with $N = 192$ at 503.17 K at monomer densities of 0.03201 (black line), 0.03296 (red line), and 0.03344 (blue line) Å^{-3}. The polymer melt is represented by four blobs. Right panel: the effective CG potential for the same polymer melt at the same state points. Inset: the attractive contribution of the effective CG potential.

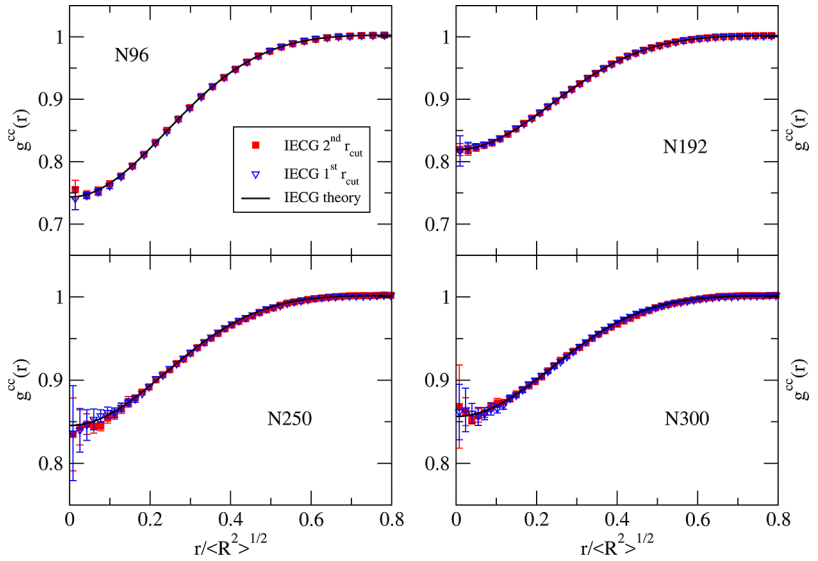

Figure 10. Theoretical and CG simulated radial distribution functions for polymers with degrees of polymerization when the polymer is represented by one soft sphere. IECG simulation results where the cutoff distances were determined over the range of $r > 0$ from the locations of the first (blue unfilled ▲) and second extrema (red filled ■) of the effective CG potential. They are compared with the IECG theoretical prediction (black —). The differences between the IECG simulation results with various treatments of potential truncation are within the statistical uncertainties (see main text).

displays the RDFs of the polymer melt represented by four blobs at various densities showing the increase in the correlation hole at higher densities, but no considerable differences in RDFs at large distances. The right panel shows the effective CG potentials at contact, $U^{bb}(0)$, which become more repulsive as the density increases. In addition, the depths of the attraction parts of the effective CG potentials and the positions of their minima increase as the density increases. Therefore, both the short-range and long-range parts of the effective potential have density dependencies.

It is useful to know how the pressure is sensitive to the choice of the end-to-end distance or the radius-of-gyration. The values of $\langle R^2\rangle/6$ and R_g^2 for the polymer melt with $N = 44$ obtained from 40 ns production period in atomistic simulations were 101 ± 1 and 123 ± 2 Å^2, respectively. However, the IECG theory predicts pressure values corresponding to R_g^2 and $\langle R^2\rangle/6$ as 847 and 848 atm, respectively. This suggests that once the value of c_0^{eff} is determined for a given state point, the pressure of the system is relatively insensitive to the values of mean-square end-to-end distance or radius-of-gyration. On the other hand, for short chain polymer melts, the structure is accurately determined with $\langle R^2\rangle/6$, while making use of R_g^2 overestimates the correlation hole, which is shown in Figure S5 in the SI.

5. POTENTIAL TRUNCATION EFFECTS

While the short-range part of the effective CG potential determines the structural consistency across variable levels of coarse-graining, the long-range part of the effective CG potential

DOI: 10.1021/acs.jpcb.7b10494
J. Phys. Chem. B 2018, 122, 3426−3440

Table 4. Calculated Pressure for Various Treatments of Potential Truncation in the IECG Simulations of Polymer Melts for Different Degrees of Polymerizations at 503 K and a Monomer Density of 0.03296 Å^{-3}[a]

Soft Sphere							
N	r_{cut1}, Å	P_{first}	$P_{first+CGcorr}$	r_{cut2}, Å	P_{second}	$P_{second+CGcorr}$	$P_{atomistic}$
96	100	597	523	186	519	523	525 ± 7
192	156	455	392	290	388	392	393 ± 6
250	188	423	362	348	357	362	362 ± 5
300	211	404	343	391	339	343	343 ± 4
Multiblobs, N = 300							
n_b	r_{cut1}, Å	P_{first}	$P_{first+CGcorr}$	r_{cut2}, Å	P_{second}	$P_{second+CGcorr}$	$P_{atomistic}$
1	211	404	343	391	339	343	343 ± 4
2	128	393	344	239	341	343	343 ± 4
4	78	381	343	147	342	343	343 ± 4
6	59	374	343	111	342	343	343 ± 4
10	41	367	346	78	346	346	343 ± 4

[a]All pressure values are reported in atm. The cutoff distances for the IECG simulations were determined over the range of $r > 0$ from the locations of the first (r_{cut1}) and second (r_{cut2}) extrema of effective CG potential. The long-range CG corrections (CGcorr) were then applied to report the CG pressures, which are in excellent agreement with the atomistic pressures. The statistical uncertainties for IECG simulations results are all less than 1 atm.

is important for consistency in thermodynamic properties. However, care is required to interpret the potential truncation in the effective CG potential. In the atomistic simulations in this work, the van der Waals interactions were explicitly calculated up to the potential truncation distance, and the long-range contributions beyond this cutoff distance may be approximated by analytical tail corrections to report the thermodynamic properties such as pressure and internal energy.[35,41] In the SI, these tail corrections are discussed for the Lennard-Jones polymer melts studied in this work. Here we focus on the corrections related to the coarse-graining procedure, where the effective CG potential has a long repulsive tail with a small attractive contribution that only appears after the RDF diminishes to 1. We investigate how the pressure and RDFs change with various treatments of the cutoff distance in the IECG method and compare them with the corresponding atomistic simulation results. Two approaches have been used. The cutoff distances for the IECG simulations were determined over the range of $r > 0$ from the locations of the first and second extrema of effective CG potential (r_{cut1} and r_{cut2} approaches, respectively). As mentioned before, all results presented in Tables 1 and 2 use the r_{cut2} approach. The IECG simulation details with the r_{cut1} approach are the same as the r_{cut2} approach except a time step of 10 fs was used for 4-blob simulations and a time step of 2 fs was used for 6- and 10-blob simulations. In addition, the neighbor skin distances of 8, 15, and 30 Å were used for 4-, 6-, and 10-blob simulations. It is important to note that the system may become unstable for relatively large time steps and/or small neighbor skin distances in this approach.

Figure 10 presents the IECG simulated RDFs for the polymer melts represented by soft spheres for the r_{cut1} and r_{cut2} approaches and compares them with the IECG theoretical results. The RDFs are statistically indistinguishable for the two approaches for polymers with various degrees of polymerizations, and both are in excellent agreement with the IECG theoretical calculations and also the atomistic simulation results as can be inferred from Figure 4. It is worth mentioning that, for the same length of trajectories, the uncertainties for the first cutoff approach are usually higher than the second cutoff approach. Similarly, Figure S6 compares the IECG simulated RDFs for the multiblob models with n_b values of 2, 4, 6, and 10 for the polymer melt with $N = 300$ for the r_{cut1} and r_{cut2} approaches. Excellent agreement is observed for the aforementioned approaches over various levels of coarse-graining. Therefore, the structure of the polymer melts can be determined from the relatively short-range repulsive CG interactions suggesting that the long-range weak attractive forces exerted on a given chain by its neighbors largely cancel.[42]

Table 4 lists the average values of the pressure for various approaches. Cutting the effective CG potential at the first cutoff distance significantly overestimates the values of the pressure in the IECG simulations because the small attraction part of the effective CG potential, which contributes negatively, is neglected. Adding the long-range CG corrections almost completely incorporates the attraction contributions. On the other hand, truncating the effective CG potential at the second cutoff distance only slightly underestimates the values of the pressure, and adding the long-range CG corrections again results in excellent agreement with the atomistic simulation results. Therefore, the effect of the relatively long-range attractive potential on the EOS of the polymer melts is merely to lower the pressure, and the attractive forces do not influence the molecular configurations.[42]

6. DISCUSSION AND CONCLUSIONS

In a CG model, the interactions are effective free energies in the CG coordinates and are thermodynamically state-dependent. Therefore, it is plausible to treat the thermodynamic variables such as density as active, which means that the density dependence of the effective interactions is regarded as an intrinsic property of the CG model. In this framework, the appropriate statistical-mechanical formalism is required in order to describe thermal equilibrium.[12] Here we have derived a CG virial, which accurately captures the density dependence of the effective CG potential. The effective CG potential is obtained starting from the Ornstein−Zernike equation for polymers,[24] while coarse-graining each macromolecule into one or more blobs, i.e., the IECG method.[19,21] The IECG method accurately computes the pressure, which reproduces the atomistic simulation results, while preserving the consistency in pair-correlation functions. The CG potential depends on two parameters, namely, the zero wave-vector limit of effective direct monomer−monomer correlation function, c_0^{eff}, and the mean-square end-to-end distance, $\langle R^2 \rangle$. The IECG method is reasonably transferable because c_0^{eff} can be determined from the

DOI: 10.1021/acs.jpcb.7b10494
J. Phys. Chem. B 2018, 122, 3426−3440

accurate EOS and $\langle R^2 \rangle$, which can be predicted by the principles of polymer physics and the related extensive works.[43−47] This is an important advantage of the IECG method when compared to the well-known CG approaches such as the iterative Boltzmann inversion (IBI)[5,48,49] and force matching[6] methods, where the parameters that are optimized for a given state point are not transferable to other state points.

A number of relevant points about coarse-graining emerged from this study. MD simulations were performed with the IECG potential at variable levels of resolution, from the soft sphere representation to the multiblob representation, and directly compared to atomistic simulations. Through a comprehensive evaluation of pressure and structure functions, both in the real and reciprocal spaces, it was shown that it is possible to find a CG potential that maintains the consistency with the atomistic description for both structure and pressure, while changing the level of coarse-graining. Furthermore, in the condition in which the MSA applies, i.e., at the liquid density, the IECG EOS and the pair distribution functions are solved analytically, providing an additional test for the validity of the results obtained from the CG simulations. The analytical solution of the IECG equation confirms again the agreement observed in the simulation results, and, in general, provides a formal method to study the theoretical implications of a CG procedure. For example, this study shows that the density dependence of the CG potential is captured in the zero wave-vector limit of the effective direct monomer−monomer correlation function. In a bottom-up CG approach, the parameter c_0^{eff} can be obtained from a proper number of atomistic simulations performed in the canonical ensemble. In a top-down IECG model, this parameter can be obtained directly from the experimental isothermal compressibility of the liquid.

It is worth noticing that the IECG method is based on a CG model that has solid foundations in the statistical mechanics of liquid. The IECG method does not necessarily require the performance of initial atomistic simulations of the system that one wants to coarse-grain.[22] We argue that this is the main advantage of the IECG method, with respect to other CG approaches, because performing atomistic simulations for every system one wants to coarse-grain in part defeats the purpose of building a CG model, which should be predictive: It is not clear what extra information can be gained from the CG simulations that is not already contained in the atomistic simulations.

The roles of short-range repulsive and long-range attractive interactions have been investigated extensively in determining the structure and thermodynamics in the CG representation. Note that, compared to the atomistic simulations, the short-range repulsive part of the effective IECG potential is much more long-ranging due to the CG procedure. It is demonstrated that, similar to the atomistic simulations, the repulsive part of the effective CG potential accurately determines the structure of the polymer melts at liquid density, and the positional correlations in the CG coordinate are due to the repulsive forces. Therefore, the CG models that idealize the attractive forces without correlating effects, but treat the correlating effects of the repulsive forces with high accuracy, should be successful in reproducing the liquid structure in the high density limit. On the other hand, following the discussion by Widom[42] we speculate that the success of CG models for investigating the critical phenomena and the character of the liquid−vapor equilibrium depends on their ability to capture the attractive part of the CG potential with great fidelity. As shown in Table 4, excluding the long-range attractive part of the effective CG potential results in significant inaccuracies in pressure. Decomposing the pressure into attractive and repulsive contributions results in

$$P = \left(\frac{\partial (TS - U_{\text{rep}} - U_{\text{att}})}{\partial V} \right)_T \approx P_{\text{rep}} - \rho_{\text{m}}^2 \frac{c_{0\text{att}}^{\text{eff}}}{2\beta} \tag{43}$$

where S is the entropy of the CG system, U_{rep} and U_{att} are the repulsive and attractive parts of the CG potential, respectively, P_{rep} is the pressure resulting from the repulsive forces, and $c_{0\text{att}}^{\text{eff}}$ is the effective monomer−monomer direct correlation function, which only contains the attractive forces, at the zero wave-vector limit. Note that the configurational entropy of the CG system with only the repulsive forces is almost identical to the configurational entropy of the CG system when both attractive and repulsive forces are included because the attractive potential is long-ranging and weak and can be conceived as a uniform background potential with no gradient. Therefore, eq 43 suggests that the effect of the uniform potential from the attractive CG forces is to lower the pressure by an amount proportional to the square of the density.

As discussed, the range of effective CG potential is much longer than the atomistic potential. In the IECG simulations, the system size is determined once the cutoff distance is calculated and the box length is usually slightly more than twice the cutoff distance. Making use of larger box lengths (system sizes) has negligible effects on the structural and thermodynamic properties presented in this work (results not shown). Therefore, cutting the CG potential at shorter distances, which is sufficient to represent the repulsive forces with high accuracy, can save significant computational time. The long-range attractive contributions of the effective CG potential can be added after IECG MD simulations to compute the thermodynamic properties while improving efficiency.[50]

The calculated EOSs in the IECG method cover very well the data points obtained by MD simulations of polymer melts. This, in turn, allows one to calculate the Helmholtz free energy of polymer melts by integrating the EOS along a reasonable reversible path (such as isotherm) using the thermodynamic integration methods as shown in a previous work.[22] A direct extension would be the application of the IECG approach to the Widom method[51] to calculate the chemical potential for polymer melts. Unlike atomistic simulations, where insertions of polymers are too inefficient for the polymer melts with long chain lengths, the CG representations are extremely efficient because the IECG potential is soft and does not suffer from the significant overlap in atomistic simulations. Therefore, a Boltzmann factor of zero, as usually occurs in the atomistic simulations, is circumvented. A similar argument can be applied to the grand canonical simulations, where successful insertions of chains are extremely rare, and thus, n is poorly sampled. Therefore, it is perceivable to implement the IECG method into the aforementioned types of simulations. In addition, the constant temperature−pressure (NPT) CG simulations require the state-dependent CG effective potential, but the CG virial should be compatible with the corresponding atomistic virial at each density. The IECG method can be extended to be used in NPT simulations by accurately incorporating the density dependence of the CG potential. This is important because, as pointed out by Andersen et al.,[52] recent CG methods are ad hoc in nature and lack a strong theoretical justification in terms of consistency of atomistic and CG ensembles.[6] In addition, these recent numerical potentials that are optimized to reproduce an atomistic quantity suffer from the problem of being not transferable to other systems or to other

DOI: 10.1021/acs.jpcb.7b10494
J. Phys. Chem. B 2018, 122, 3426−3440

thermodynamic conditions.[52] Furthermore, the IECG can be incorporated in mixed resolution modeling, where maintaining consistency between the resolution levels is not trivial in Adaptive Resolution Simulations (AdResS).[53−55] In the Force AdResS scheme, a general Hamiltonian formulation is impeded due to the enforcement of Newton's third law, while in the Hamiltonian AdResS scheme the drift forces that appear in the hybrid region should be corrected.[54] Therefore, in the present state of development of the method, the degree of consistency of the AdResS depends both on the type of AdResS approach that is chosen and on the compatibility of the different models adopted in the regions that have different resolution. The AdResS schemes can take advantage of the IECG theory because the related thermodynamical and structural properties are conserved in the IECG method[19,20] and the ad hoc forces in the AdResS schemes that balance the CG with the atomistic parts can be minimized.

The present work has focused on the density as an active variable in the effective CG potential, but similar issues exist concerning the temperature dependence of the effective CG potential. This is especially important in the simulations/analyses in microcanonical ensembles, but even in the canonical ensemble as discussed by Stillinger et al.,[11] the thermodynamic energies for such effective potentials involve additional terms. For instance, for the multiblob models discussed in this work, the thermodynamic intermolecular energies are given by

$$\frac{\langle U^{\text{inter}}\rangle}{n} = \frac{\rho_b n_b}{2}\int\left[U^{bb}(r,\beta,\rho_b,N) + \beta\frac{\partial U^{bb}(r,\beta,\rho_b,N)}{\partial\beta}\right]g^{bb}(r,\beta,\rho_b,N)\,\mathrm{d}\mathbf{r} \tag{44}$$

but this is another feature whose full analysis should await a later examination.

■ ASSOCIATED CONTENT

Supporting Information

The Supporting Information is available free of charge on the ACS Publications website at DOI: 10.1021/acs.jpcb.7b10494.

Derivation of equation of state, simulation protocols, and data analysis (PDF)

■ AUTHOR INFORMATION

Corresponding Author

*E-mail: mguenza@uoregon.edu.

ORCID

Marina G. Guenza: 0000-0002-1151-4766

Notes

The authors declare no competing financial interest.

■ ACKNOWLEDGMENTS

This work was supported by the National Science Foundation (NSF) Grant CHE-1362500. CPU time was provided by NSF Grant ACI-1053575 through Extreme Science and Engineering Discovery Environment (XSEDE) resources. We are grateful to Paula J. Seeger for reading/editing the manuscript.

■ REFERENCES

(1) Schweizer, K. S.; Curro, J. G. Integral Equation Theories of the Structure, Thermodynamics, and Phase Transitions of Polymer Fluids. *Adv. Chem. Phys.* **1997**, *98*, 1−142.

(2) Peacock, A. J. *Handbook of Polyethylene: Structures, Properties, and Applications*; Marcel Dekker: New York, 2000.

(3) Santangelo, G.; Di Matteo, A.; Müller-Plathe, F.; Milano, G. From Mesoscale Back to Atomistic Models: A Fast Reverse-mapping Procedure for Vinyl Polymer Chains. *J. Phys. Chem. B* **2007**, *111*, 2765−2773.

(4) Dunn, N. J.; Noid, W. G. Bottom-up Coarse-grained Models that Accurately Describe the Structure, Pressure, and Compressibility of Molecular Liquids. *J. Chem. Phys.* **2015**, *143*, 243148.

(5) Reith, D.; Pütz, M.; Müller-Plathe, F. Deriving Effective Mesoscale Potentials from Atomistic Simulations. *J. Comput. Chem.* **2003**, *24*, 1624−1636.

(6) Izvekov, S.; Voth, G. A. Multiscale Coarse Graining of Liquid-State Systems. *J. Chem. Phys.* **2005**, *123*, 134105.

(7) Hsu, D. D.; Xia, W.; Arturo, S. G.; Keten, S. Thermomechanically Consistent and Temperature Transferable Coarse-graining of Atactic Polystyrene. *Macromolecules* **2015**, *48*, 3057−3068.

(8) Johnson, M. E.; Head-Gordon, T.; Louis, A. A. Representability Problems for Coarse-grained Water Potentials. *J. Chem. Phys.* **2007**, *126*, 144509.

(9) Montes-Saralegui, M.; Kahl, G.; Nikoubashman, A. On the Applicability of Density Dependent Effective Interactions in Cluster-forming Systems. *J. Chem. Phys.* **2017**, *146*, 054904.

(10) Zhang, Z.; Pfaendtner, J.; Grafmüller, A.; Voth, G. A. Defining Coarse-grained Representations of Large Biomolecules and Biomolecular Complexes from Elastic Network Models. *Biophys. J.* **2009**, *97*, 2327−2337.

(11) Stillinger, F. H. Effective Pair Interactions in Liquids. Water. *J. Phys. Chem.* **1970**, *74*, 3677−3687.

(12) Stillinger, F. H.; Sakai, H.; Torquato, S. Statistical Mechanical Models with Effective Potentials: Definitions, Applications, and Thermodynamic Consequences. *J. Chem. Phys.* **2002**, *117*, 288−296.

(13) Ascarelli, P.; Harrison, R. J. Density-Dependent Potentials and the Hard-Sphere Model for Liquid Metals. *Phys. Rev. Lett.* **1969**, *22*, 385−388.

(14) Hansen, J. P.; McDonald, I. R. *Theory of Simple Liquids*; Academic Press: Amsterdam, 2003.

(15) Schweizer, K. S.; Curro, J. G. Integral-Equation Theory of the Structure of Polymer Melts. *Phys. Rev. Lett.* **1987**, *58*, 246−249.

(16) Yatsenko, G.; Sambriski, E. J.; Nemirovskaya, M. A.; Guenza, M. Analytical Soft-core Potentials for Macromolecular Fluids and Mixtures. *Phys. Rev. Lett.* **2004**, *93*, 257803.

(17) Yatsenko, G.; Sambriski, E. J.; Guenza, M. G. Coarse-grained Description of Polymer blends as Interacting Soft-Colloidal Particles. *J. Chem. Phys.* **2005**, *122*, 054907.

(18) Clark, A. J.; Guenza, M. G. Mapping of Polymer Melts onto Liquids of Soft-Colloidal Chains. *J. Chem. Phys.* **2010**, *132*, 044902.

(19) Clark, A. J.; Mccarty, J.; Lyubimov, I. Y.; Guenza, M. G. Thermodynamic Consistency in Variable-Level Coarse Graining of Polymeric Liquids. *Phys. Rev. Lett.* **2012**, *109*, 168301.

(20) McCarty, J.; Clark, A. J.; Lyubimov, I. Y.; Guenza, M. G. Thermodynamic Consistency between Analytic Integral Equation Theory and Coarse-grained Molecular Dynamics Simulations of Homopolymer Melts. *Macromolecules* **2012**, *45*, 8482−8493.

(21) Clark, A. J.; McCarty, J.; Guenza, M. G. Effective Potentials for Representing Polymers in Melts as Chains of Interacting Soft Particles. *J. Chem. Phys.* **2013**, *139*, 124906.

(22) McCarty, J.; Clark, A. J.; Copperman, J.; Guenza, M. G. An Analytical Coarse-graining Method which Preserves the Free Energy, Structural Correlations, and Thermodynamic State of Polymer Melts from the Atomistic to the Mesoscale. *J. Chem. Phys.* **2014**, *140*, 204913.

(23) Krakoviack, V.; Hansen, J. P.; Louis, A. A. Relating Monomer to Centre-of-Mass Distribution Functions in Polymer Solutions. *Europhys. Lett.* **2002**, *58*, 53−59.

DOI: 10.1021/acs.jpcb.7b10494
J. Phys. Chem. B 2018, 122, 3426−3440

(24) Schweizer, K. S.; Curro, J. G. RISM Theory of Polymer Liquids: Analytical Results for Continuum Models of Melts and Alloys. *Chem. Phys.* **1990**, *149*, 105−127.
(25) Flory, P. J. *Principles of Polymer Chemistry*; Cornell University Press: Ithaca, 1953.
(26) Go, N.; Scheraga, H. A. On the Use of Classical Statistical Mechanics in the Treatment of Polymer Chain Conformation. *Macromolecules* **1976**, *9*, 535−542.
(27) Honnell, K. G.; Hall, C. K.; Dickman, R. On the Pressure Equation for Chain Molecules. *J. Chem. Phys.* **1987**, *87*, 664−674.
(28) Karplus, M.; Kushick, J. N. Method for Estimating the Configurational Entropy of Macromolecules. *Macromolecules* **1981**, *14*, 325−332.
(29) Laso, M.; Öttinger, H. C.; Suter, U. W. Bond-length and Bond-angle Distributions in Coarse-grained Polymer Chains. *J. Chem. Phys.* **1991**, *95*, 2178−2182.
(30) Louis, A. A.; Bolhuis, P. G.; Hansen, J. P.; Meijer, E. J. Can Polymer Coils Be Modeled as "Soft Colloids"? *Phys. Rev. Lett.* **2000**, *85*, 2522−2525.
(31) Biben, T.; Hansen, J. P. Phase Separation of Asymmetric Binary Hard-Sphere Fluids. *Phys. Rev. Lett.* **1991**, *66*, 2215−2218.
(32) Dinpajooh, M.; Guenza, M. G. Thermodynamic Consistency in the Structure-based Integral Equation Coarse-grained method. *Polymer* **2017**, *117*, 282−286.
(33) Plimpton, S. Fast Parallel Algorithms for Short-Range Molecular Dynamics. *J. Comput. Phys.* **1995**, *117*, 1−19.
(34) Mei, J.; Davenport, J. W.; Fernando, G. W. Analytic Embedded-atom Potentials for FCC Metals: Application to Liquid and Solid Copper. *Phys. Rev. B: Condens. Matter Mater. Phys.* **1991**, *43*, 4653−4658.
(35) Allen, M. P.; Tildesley, D. J. *Computer Simulations of Liquids*; Oxford University Press: Oxford, 1987.
(36) Thompson, A. P.; Plimpton, S. J.; Mattson, W. General Formulation of Pressure and Stress Tensor for Arbitrary Many-body Interaction Potentials under Periodic Boundary Conditions. *J. Chem. Phys.* **2009**, *131*, 154107.
(37) Strobl, G. R. *The Physics of Polymers: Concepts for Understanding their Structure and Behavior*, 2nd ed.; Springer: Berlin, 1997.
(38) McCarty, J.; Lyubimov, I. Y.; Guenza, M. G. Multiscale Modeling of Coarse-grained Macromolecular Liquids. *J. Phys. Chem. B* **2009**, *113*, 11876−11886.
(39) Peters, J. H.; Klein, R.; Delle Site, L. Simulation of Macromolecular Liquids with the Adaptive Resolution Molecular Dynamics Technique. *Phys. Rev. E: Stat. Phys., Plasmas, Fluids, Relat. Interdiscip. Top.* **2016**, *94*, 023309.
(40) Carnahan, N. F.; Starling, K. E. Thermodynamic Properties of a Rigid-Sphere Fluid. *J. Chem. Phys.* **1970**, *53*, 600−603.
(41) Frenkel, D.; Smit, B. *Understanding Molecular Simulations*, 2nd ed.; Academic Press: San Diego, 2002.
(42) Widom, B. Intermolecular Forces and the Nature of the Liquid State. *Science* **1967**, *157*, 375−382.
(43) Debye, P.; Bueche, F. Distribution of Segments in a Coiling Polymer Molecule. *J. Chem. Phys.* **1952**, *20*, 1337−1338.
(44) Hsu, H.-P.; Kremer, K. Static and Dynamic Properties of Large Polymer Melts in Equilibrium. *J. Chem. Phys.* **2016**, *144*, 154907.
(45) Grayce, C. J.; Yethiraj, A.; Schweizer, K. S. Liquid-state Theory of the Density Dependent Conformation of Nonpolar Linear Polymers. *J. Chem. Phys.* **1994**, *100*, 6857−6872.
(46) Tsolou, G.; Stratikis, N.; Baig, C.; Stephanou, P. S.; Mavrantzas, V. G. Melt Structure and Dynamics of Unentangled Polyethylene Rings: Rouse Theory, Atomistic Molecular Dynamics Simulation, and Comparison with the Linear Analogues. *Macromolecules* **2010**, *43*, 10692−10713.
(47) Ramos, J.; Vega, J. F.; Martinez-Salazar, J. Molecular Dynamics Simulations for the Description of Experimental Molecular Conformation, Melt Dynamics, and Phase Transitions in Polyethylene. *Macromolecules* **2015**, *48*, 5016−5027.
(48) Wang, H.; Junghans, C.; Kremer, K. Comparative Atomistic and Coarse-grained Study of Water: What Do We Lose by Coarse-graining? *Eur. Phys. J. E: Soft Matter Biol. Phys.* **2009**, *28*, 221−229.
(49) Agrawal, V.; Arya, G.; Oswald, J. Simultaneous Iterative Boltzmann Inversion for Coarse-graining of Polyurea. *Macromolecules* **2014**, *47*, 3378−3389.
(50) Ozog, D.; McCarty, J.; Gossett, G.; Malony, A. D.; Guenza, M. Fast Equilibration of Coarse-grained Polymeric Liquids. *J. Comput. Sci.* **2015**, *9*, 33−38.
(51) Widom, B. Potential-distribution Theory and the Statistical Mechanics of Fluids. *J. Phys. Chem.* **1982**, *86*, 869−872.
(52) Das, A.; Andersen, H. C. The Multiscale Coarse-graining Method. V. Isothermal-Isobaric Ensemble. *J. Chem. Phys.* **2010**, *132*, 164106.
(53) Praprotnik, M.; Poblete, S.; Kremer, K. Statistical Physics Problems in Adaptive Resolution Computer Simulations of Complex Fluids. *J. Stat. Phys.* **2011**, *145*, 946−966.
(54) Potestio, R.; Fritsch, S.; Espanol, P.; Delgado-Buscalioni, R.; Kremer, K.; Everaers, R.; Donadio, D. Hamiltonian Adaptive Resolution Simulation for Molecular Liquids. *Phys. Rev. Lett.* **2013**, *110*, 108301.
(55) Guenza, M. G. Advancements in Multi Scale Modeling: Adaptive Resolution Simulations and Related Issues. *Eur. Phys. J.: Spec. Top.* **2015**, *224*, 2491−2495.

DOI: 10.1021/acs.jpcb.7b10494
J. Phys. Chem. B 2018, 122, 3426−3440